Multifractal spatial distribution of epilithic microphytobenthos on a Mediterranean rocky shore

*Martina Dal Bello[1], Elena Maggi[1], Luca Rindi[1], Antonella Capocchi[2], Debora Fontanini[2], Carlos Sanz-Lazaro[1,3], Lisandro Benedetti-Cecchi[1]

[1]Dipartimento di Biologia, Università di Pisa, CoNISMa, Via Derna 1, I-56126 Pisa, Italy (emaggi@biologia.unipi.it, lrindi@biologia.unipi.it, lbenedetti@biologia.unipi.it)

[2]Dipartimento di Biologia, Università di Pisa, Via L. Ghini 5, I-56126 Pisa, Italy (acapocchi@biologia.unipi.it, dfontanini@biologia.unipi.it)

[3]Present address: Departamento de Ciencias del Mar y Biología Aplicada, Universidad de Alicante, PO Box 99, E-03080 Alicante, Spain (carsanz@ua.es)

* Corresponding author

Email: mdalbello@biologia.unipi.it

Tel. +39 050 221415

Fax. +39 050 2211410

Understanding how patterns and processes relate across spatial scales is one of the major goals in ecology. 1/*f* models have been applied mostly to time series of environmental and ecological variables, but they can also be used to analyse spatial patterns. Since 1/*f* noise may display scale-invariant behaviour, ecological phenomena whose spatial variability shows 1/*f* type scaling are susceptible to further characterization using fractals or multifractals. Here we use spectral analysis and multifractal techniques (generalized dimension spectrum) to investigate the spatial distribution of epilithic microphytobenthos (EMPB) on rocky intertidal surfaces. EMPB biomass was estimated from calibrated colour-infrared images that provided indirect measures of rock surface chlorophyll *a* concentration, along two 8m and one 4m long transects sampled in January and November 2012. Results highlighted a pattern of spectral coefficient close to or greater than one for EMPB biomass distribution and multifractal structures, that were consistent among transects, implying scale-invariance in the spatial distribution of EMPB. These outcomes can be interpreted as a result of the superimposition of several biotic and abiotic processes acting at multiple spatial scales. However, the scale-invariant nature of EMPB spatial patterns can also be considered a hallmark of self-organization, underlying the possible role of scale-dependent feedback in shaping EMPB biomass distribution.

The measurement of variability in population abundance and distribution followed by the identification of the underlying causes are major goals in ecology (Denny et al. 2004). Hierarchical sampling designs, combined with variance components estimates, have been extensively employed to examine spatial patterns in abundance of animal and plant populations, showing how most of the variation is concentrated at small scales (Fraschetti et al. 2005, Meyer 2006). These methods focus on discrete spatial scales and require decisions to be made about the number, extent and spacing of the scales investigated. A possible limitation of this approach is that important scales of variation may be omitted from the study. The major strength of hierarchical sampling designs is that they enable the simultaneous analysis of a broad range of scales and they are the only possible approach to compare biogeographic or continental scales or when the habitat of interest (e.g., rocky shores) is interspersed among unfavourable habitats (e.g., sandy beaches). The alternative approach of sampling continuously in space is simply impractical in these circumstances.

Examining spatial variation in ecological variables continuously in space may, however, capture patterns of variability that could go undetected otherwise. For example, Denny et al. (2004) quantified spatial variation of physical and biological variables sampling continuously along three intertidal transects tens to hundreds of meters in length, on a wave-swept rocky shore at Hopkins Marine Station (CA). Results contradicted the expectation that variability is concentrated mostly at small spatial scales and the existence of a characteristic scale of variability. In contrast, using spectral analysis, these authors found a continuous increase of variance with the scale of observation, a pattern that was well described by $1/f$-noise models. One of the key findings of this work was that, for several of the variables analyzed, patterns of distribution were adequately described by a power law with a spectral coefficient close to one. These patterns are usually referred to as 'pink noise' and underscore variability at all the scales analyzed, suggesting that multiple processes affect the response variable of concern.

Pink noise patterns of variability can be further characterized using fractals (Halley and Incausti 2004). Mandelbrot (1983) coined the term "fractal" to designate objects with fractional or a

58 non integer number of dimensions, that display self-similarity across a range of spatial scales of
59 observations. Fractal methods have been applied to various natural phenomena, including patterns
60 in surface topography (Commito and Rusignuolo 2000), blood networks (Yang and Wang 2013),
61 climatic variation (Bodai and Tel 2012), earthquakes (Malamud and Turcotte 1999) and fires
62 (Abaimov et al. 2007). All these phenomena are usually described by one estimated fractal
63 dimension *D*, which measures the object's capacity to fill the space. In some cases, however, the
64 description of particular natural events requires not one, but a set of fractal dimensions. These
65 phenomena are better characterized by multifractals, which can be seen as sets of interweaved
66 fractals with different dimensions (Stanley and Meakin 1988). Multifractals are useful for the
67 description of the spatial (or temporal) organization of population abundance or biomass for which
68 complex patterns are expected (Halley et al. 2004). Multifractality is attributed to long-range
69 correlations and thus should be expected in the presence of 1/*f* noise spatial (or temporal) patterns
70 (Stanley and Meakin 1988). Moreover, multifractal analysis provides a complementary approach to
71 spectral analysis. While spectral analysis examines the relative contribution of different spatial or
72 temporal scales to total variance and may detect scale-invariant patterns, multifractals evaluate
73 whether scaling relations change according to the spatial or temporal resolution of observations.
74 Overall, 1/*f* noise and multifractality are related to the extent that both patterns may reflect the
75 juxtaposition of multiple independent processes (Kendal 2013). However, the combined action of
76 multiple processes is not the only mechanism involved in the formation of power law distributions.
77 Borda-de-Água and co-authors (2007), simulating the spatial distribution of model tree species,
78 found that multifractals may also originate from Lévy flight dispersal patterns, with long distance
79 events being frequent enough to generate a fat tail in the frequency distribution of dispersal
80 distances.

81 Epilithic microphytobenthos (EMPB) forming biofilms on rocky shores are ubiquitous
82 worldwide and consist primarily of photosynthetic organisms, such as diatoms, cyanobacteria and
83 macroalgal spores and germlings (Hill and Hawkins 1991). Biofilms play important functional roles

84 on rocky intertidal shores, facilitating the attachment of algal propagules and the settlement of
85 larvae of many sessile invertebrates (Rodriguez et al. 1993) and providing food for grazing
86 gastropods (Underwood 1984). EMPB constitutes the major fraction of biomass produced and
87 directly consumed on a rocky shore (Thompson et al. 2000).

88 EMPB offer unique opportunities to investigate the spatial ecology of rocky shore populations.
89 The microscopic size of constituting organisms enables the analysis of a broad range of tractable
90 scales, from very small (mm) to very large (tens to hundreds of meters) for the organisms of
91 concern. Recent advances in field-based remote sensing, in particular colour-infrared imagery
92 (CIR), have significantly improved our ability to obtain *in situ* quantitative measures of chlorophyll
93 *a* (a proxy for EMPB biomass) enabling the collection of large amount of data at a fine spatial
94 resolution and over a range of several, continuous spatial scales (Murphy et al. 2006). Hence data
95 can be analyzed across the entire range of spatial scales within the boundary of an image or a set of
96 consecutive images and the relative positions of observations are implicitly stored within the images
97 (Murphy et al. 2009).

98 Notwithstanding rapid technological progress enabling efficient sampling of intertidal biofilms,
99 to date only one study has examined variability of EMPB at multiple spatial scales (Murphy et al.
100 2008). Using a hierarchical sampling design and block mean square analysis, Murphy et al. (2008)
101 showed how variability in EMPB biomass was low at small spatial scales (block sizes from 0.002 to
102 2.26 cm^2), but increased with increasing block-size up to the largest scale examined (36.19 cm^2).
103 Because variation increased with the scale of observation and different processes were invoked to
104 explain these patterns, the results of Murphy et al. (2008) may indeed underscore $1/f$ noise process
105 and, possibly, multifractal structure in EMPB distribution. Indeed, multifractals have been detected
106 in a study on the spatial distribution of soft bottom microphytobenthos (Seuront and Spilmont 2002)
107 and in a periphyton community at different stages of succession in experimental tanks (Saravia et al.
108 2012). In particular, Saravia and co-authors, found that scale invariance arose at each stage of
109 succession, thus highlighting a temporally consistent scale-invariant behaviour that was ascribed to

self-organization. In this paper we examine spatial variation in EMPB biomass on rocky intertidal shores in the Northwest Mediterranean by means of colour-infrared imagery. From the results of previous studies on the spatial distribution of microphytobenthos (Seuront and Spilmont 2002, Murphy et al. 2008, Saravia et al. 2012) we test the following hypotheses: (1) the spectral decomposition of spatial variance in EMPB abundance follows a power law; (2) the distribution of EMPB in 2-dimensional space is multifractal. We test these hypotheses applying spectral analysis and multifractal geometry to nearly-continuous spatial EMPB data under natural field conditions.

Methods

Study system

The study was done along the coast of Calafuria (Livorno, 43°30′ N, 10°19′ E) between January and November 2012. The coast is composed of gently sloping sandstone platforms with high-shore levels (0.3-0.5 m above mean low-level water) characterized by assemblages of barnacles interspersed among areas of seemingly bare rock, where EMPB develops. Calafuria's EMPB assemblages prevalently comprise cyanobacteria and diatoms. At this height on the shore, the main grazers are the littorinid snails *Melarhaphe neritoides* (L.), which aggregate in pits and crevices when the substratum is dry and forage during sea storms and rain events (Skov et al. 2010 and references therein). The only other grazer that can occasionally forage at these heights of the shore is the limpet *Patella rustica* (L.).

In situ estimates of chlorophyll *a*

Following the image-based method proposed by Murphy et al. (2006), chlorophyll *a*, which is used as a proxy for biofilm biomass, was estimated from a ratio of reflectance at near-infrared (NIR) and red bands (Jordan 1969). The NIR:red ratio (Ratio Vegetational Index - RVI) detects the absorption of chlorophyll *a* using the reflectance at NIR wavelengths, where chlorophyll *a* does not absorb, normalized by the reflectance at red wavelengths (corresponding to the peak of chlorophyll *a* absorbance) (Murphy et al. 2006).

Here we used a particular IR-sensible camera (ADC, Tetracam Inc.), commonly employed in agricultural and vegetational studies, to obtain chlorophyll *a* estimates. The ADC is a single sensor digital camera designed and optimized to capture visible light wavelengths longer than 520 nm and near-infrared wavelengths up to 920 nm. This camera uses a Bayern-pattern filter to produce a 3-layered photo comprising green, red and NIR layers which are analogous to the red, green and blue layers produced by conventional digital cameras. The ADC system writes a greyscale RAW file for every photo; hence every photo has been colour-processed and recorded in TIFF format, using the program PixelWrench 2, prior to further use (Agricultural Camera User's Guide 2010). Photos are 2560 by 1926 pixels in size and cover an area of ground of about 52 x 35 cm. The approximate spatial resolution of each pixel is 0.2 mm.

In order to get the best focus, photos were acquired using a stable platform 60 cm above and normal to the rock surface. Different exposure times for each photo were selected depending on ambient light conditions, in order to produce bright but not saturated photos. To calibrate pixel values to the varying light conditions and different camera settings, a reflectance standard of 30% reflective Spectralon®, representing the range of brightness of Calafuria rock surfaces with microalgae, was always placed within the field of view of the camera. The calibration of data to reflectance is obtained normalizing pixel values of each band to the brightness of pixels over the standard (see Supplementary material Appendix 1).

All methods of collecting remotely sensed data require calibration/validation by comparison with direct measurements (Murphy et al. 2005). In order to calibrate/validate estimates of chlorophyll *a* derived from the ADC data, 100 rock chips ~2 cm in diameter were removed by cutting the rock with a diamond corer powered by a petrol driller and then photographed using the ADC camera. Rock chips were then taken to the laboratory for the determination of the amount of chlorophyll *a*, which was extracted in methanol as in Thompson et al. 1999. Laboratory measurements of chlorophyll *a* were related to ADC estimates (RVI index) using least squares linear regression.

161 **Sampling and data analysis**

162 Spatial patterns of EMPB abundance were investigated along two 8m transects and one 4m transect
163 about 50m from each other, yielding 18 and 9 ADC photos per transect, respectively. Sampling was
164 repeated in January and November 2012.

165 The photographs obtained from each individual transect were stitched to form a composite
166 image using a photogrammetric software (Kolor Autopano Giga 2.6). The area of the rock included
167 in each individual photo was delimited with white chalk at its corners before sampling. Adjacent
168 photos overlapped at their margins and the region of overlap was indicated by the white chalk
169 marks. This procedure facilitated the alignment of photos in the composite image, but resulted in
170 non-continuous spatial series of data because spurious chlorophyll *a* values can originate from the
171 interpolation method (nearest neighbour) used by the photogrammetric software to merge pixels in
172 the regions of overlap. Three series of observations were extracted from each composite image,
173 where a series consisted of a set of points one pixel in height and arranged along a common 'y'
174 coordinate (Fig. 1B). Each series had gaps corresponding to the areas in which adjacent photos
175 overlapped; for each series, the size of gaps was determined by measuring the distance in pixels
176 between each set of continuous points in the composite image (grey lines in Fig. 1B). The extracted
177 data were then processed with a java-routine in the ImageJ program in order to quantify NIR/red
178 ratios (the RVI index) that were then transformed into estimates of chlorophyll *a* concentration at
179 the pixel scale. Pixel per pixel calibration to reflectance is part of this routine (Supplementary
180 materials Appendix 1).

181 We used spectral analysis on linearly detrended data for each spatial series of chlorophyll *a*
182 estimates to characterize the spatial patterns of variation in EMPB biomass along each series of data
183 within each transect. Although our series were unevenly spaced, knowing the size of gaps enabled
184 us to use the Lomb-Scargle algorithm (Lomb 1976, Scargle 1982) modified by Press et al. (1992)
185 for spectral analysis. Spectral densities were estimated between the fundamental and the Nyquist
186 frequency. The fundamental frequency is defined as $1/x_{max}$, where x_{max} is the maximum spatial

extent of the data, corresponding to transects of either 4 or 8 m in our study. The Nyquist frequency is defined as $1/2\Delta x$, where Δx is the average distance between the irregularly spaced sampling points. We smoothed the periodogram with Hamming window = 10, thus minimizing the loss of information at higher frequencies (Chatfield 2004). The spectral density estimate for each series, $S(f)$, was then plotted against frequency of observation on a natural log-log scale and the spectral coefficient (β) was determined as the slope of the regression changed of sign (e.g., Denny et al. 2004). βs were estimated within the range of frequencies that displayed a $1/f$ noise pattern: the Nyquist and -7 (on the natural logarithm scale). We truncated the series at -7 because at larger spatial scales (lower frequencies) the spectral densities deviated from a $1/f$ noise pattern, becoming more similar to an autoregressive process. This behaviour possibly reflected the decreasing number of observations available to estimate spectral densities with increasing scale of observation.

The previous analysis used EMPB biomass values at the resolution of the pixel that were calibrated against laboratory measurements of chlorophyll concentration obtained from sandstone cores with areas corresponding to approximately 6400 pixels. This mismatch between the resolution at which the RVI and chlorophyll measurements were obtained might lead to biased estimates of spectral coefficients due to error propagation and the noise generated by the camera. To asses this potential bias we performed a further spectral analysis on nearly continuous spatial series of EMPB biomass data obtained from non-overlapping quadrats of 80 x 80 pixels (6400 pixels) extracted from the stitched image of each transect along a common y coordinate. The average spectral coefficients obtained for each transect with the two methods were then compared with a paired t-test.

To test the hypothesis that the spatial distribution of EMPB was multifractal, a total of 39 plots of 1024 by 1024 pixels each (approximately 400 cm^2) were selected from all the transects and processed with the java-routine on ImageJ program to obtain EMPB biomass estimates for each pixel. This plot size was chosen to match as closely as possible the range of scales employed in the

212 spectral analysis, where the largest scale of -7 corresponded to about 1096 pixels in length.
213 Multifractal geometry was determined following the method proposed by Saravia *et al*. (2012) to
214 estimate the generalized dimensions spectrum D_q of each plot (see Supplementary material
215 Appendix 2 for formulae and details of calculation). D_q is related to the spatial arrangement of
216 biomass, computed in the algorithm as the partition function Z_q, and reflects the patterns of change
217 that occur when zooming in or out from each plot by steps of size ε. The exponent q in the
218 algorithm (chosen by the investigators) captures spatial variation in high or low values of biomass
219 depending on its value (here, we used q values from -20 to +20). When q is a relatively large
220 positive number, D_q reflects the spatial patterns of large biomass values (chlorophyll a > 1 μg/cm^2),
221 whereas when q is a large negative number, D_q describes the spatial pattern of small biomasses
222 (chlorophyll a estimates between 0 and 1 μg/cm^2).
223 For multifractal objects, the spectrum of generalized dimensions D_q (not to be confounded
224 with the power spectrum) takes the shape of a sigmoid curve and it is a decreasing function of q
225 (Grassberger 1983). For mono- or non-fractal objects the spectrum is a non decreasing function of
226 q. The other assumption that must be met for the biomass distribution to be multifractal is that the
227 relationship log(Z_q) versus log(ε) should be linear for all the q used in the calculation of D_q (see
228 Supplementary material Appendix 2).
229 Deviations from spatially homogeneous biomass distributions are quantified as positive and
230 negative deviations from 2 (the expected value of the exponent of a non-fractal 2D space), for low
231 and high biomass values respectively. A plot with high peaks of biomass will have increasingly
232 lower D_q for positive q and a plot with sharp collapses of biomass will have increasingly larger D_q
233 for negative q. A plot with both peaks and falls will show large deviations from 2 (Saravia et al.
234 2012).
235 To further characterize spatial patterns of EMPB distribution we examined how D_1 varied
236 along transects, sampling dates and potentially important environmental drivers. D_1 is directly
237 related to Shannon entropy and can be thought as the decrease in information content when

238 increasing box size in the box counting method (Mendoza et al. 2010). Large values of D_1 indicate
239 greater homogeneity with increasing box size, while low values indicate the opposite. To obtain
240 reasonably long spatial series of D_1 values along transects, we repeated the multifractal geometry
241 analysis described above using plots of 128 x 128 (instead of 1024 x 1024) pixels from the two 8m
242 transects. These plots were aligned along a common 'y' coordinate along composite images and the
243 size of gaps was recorded as the number of missing 128 x 128 plots in the regions of overlap
244 between adjacent photos (Fig. 1C). This yielded a series of 64 D_1 values for each 8m transect and
245 sampling date. We analysed these data in two ways. First, we used a mixed-effect model including
246 the main effects and interactions among densities of grazers (the littorinid *Melaraphe neritoides*),
247 and average rainfall in the week before sampling in the fixed part of the model, and transects as a
248 grouping factor with a random intercept. Densities of grazers were calculated within each individual
249 image of the composite transects, whereas daily precipitation data were obtained from Lamma
250 Toscana (http://www.lamma.rete.toscana.it/). Rainfall and aerial temperature were the two of most
251 obvious environmental variables discriminating between sampling dates. The daily values of these
252 variables were highly correlated in the week before sampling (r=0.9, n=7), so we used only rainfall
253 in the analysis because this variable has been related to the activity of grazers in previous studies
254 (Bates and Hicks 2005, Skov et al. 2010).
255 Following the results of the mixed effect model, which highlighted a significant grazer x
256 rainfall interaction (see Results), we examined the cross-correlation between D_1 and density of
257 grazers along each transect at each date of sampling. We used the function spline.correlog in the R
258 package 'ncf' for this analysis (Bjornstad and Falck 2001).
259 All analyses were performed in R 2.15.2. (R Development core team 2012).

260 ## Results

There was a strong linear relation between chlorophyll *a* estimates obtained with laboratory extraction methods and the RVI index (Fig. 2; R^2= 0.80, SE=0.12, p<0.001, n=100), indicating that ADC images can be used to predict EMPB abundance.

Variance of chlorophyll *a* concentration was inversely related to the frequency of observation for all the spatial series investigated, (see Appendix 3 Fig. A3.1 and A3.2). Spectral coefficients ranged from 0.95 to 1.64 (mean 1.34), indicating a predominance of "red-noise" spectra (Table 1). The analysis based on quadrats of 80 x 80 pixels yielded very similar results to those obtained from the analysis of series of individual pixels, with spectral coefficients in the range 0.86 -1.7 that were still indicative of 'red-noise' spatial patterns (Table A4.1, Supplementary material Appendix 4). The paired *t*-test did not highlight statistically significant differences in mean spectral coefficients between scales calculated at the transect level (t=-1.36, P>0.23, with five degrees of freedom).

EMPB biomass displayed multifractal spatial distribution in all plots of 1024 x 1024. The theoretical prediction that D_q should be a monotonically decreasing function of q was supported in all cases (Fig. 3) and the linear relation necessary for the biomass distribution to be multifractal was achieved for all the plots sampled and all the values for q used to calculate the spectrum of generalized dimensions (R^2 were larger than 0.99 in all cases) (see Supplementary material Appendix 2, Fig. A2.1).

Multifractal spatial distribution of EMPB biomass also emerged from the analysis of the plots of 128 x 128 pixels (data not shown). The analysis of the resulting D_1 values highlighted a statistically significant interactive effect of the density of snails and the average rainfall in the week before sampling (Table 2). D_1 decreased with increasing density of grazers under dry meteorological conditions, whereas the opposite was observed under wet conditions (Fig. 4).

The spatial correlograms showed a positive relation between D_1 and littorinid density at small spatial scales for all combinations of transects and sampling dates (Fig. 5). Positive cross-

correlation was also evident at the largest spatial scale in one of the two transects sampled in November 2012 (Fig. 5).

Discussion

We found a strong linear relation between laboratory chlorophyll *a* estimates and the RVI index. The regression model explains 80% of variability in the data. Microscopic variations in colour and topography of the surface of sandstone rock cores, together with occasional small areas of specular reflectance likely accounted for some of the remaining 20% of unexplained variability (Murphy et al. 2009).

Our results support the hypothesis that EMPB biomass is distributed according to a power law and that multifractal organization characterizes EMPB spatial distribution. Spectral coefficients for all the series of observations taken along linear transects were close to or greater than one. Expanding the analysis in a two-dimensional space through multifractal geometry produced an analogous outcome. Multifractal analysis, indeed, indicated that the spatial distribution of EMPB was characterized by a combination of several fractal sets with different fractal dimensions. The scale-invariant nature of EMPB biomass distribution suggests the superimposition of several abiotic and biotic processes operating at different spatial scales (Hausdorff and Peng 1996). Positive and negative biotic interactions are likely to be responsible for the variability observed at the smallest spatial scales (from millimetres to centimetres). For example, the production of extracellular polymeric substances (EPS) has been described as a mechanism of facilitation between microalgal cells that may promote the development of EMPB patches, through reducing desiccation, favouring nutrient retention and providing protection from UV radiations (Potts 1999). However, within EMPB patches mechanisms of facilitation could be counterbalanced by competitive interactions for resources such as light, nutrients and space among microalgae. These mechanisms of facilitation and competition may further interact with the microtopography of substratum, which may also have a multifractal structure (Commito and Rusignuolo 2000) and can promote variation in important

310 variables for EMPB growth, such as solar radiation, ground temperature and moisture (Murphy et
311 al. 2008). For example, the presence of small pits and crevices on the rock favours water retention,
312 providing a surrounding halo of favourable conditions for the development of EMPB (Jackson et al.
313 2013).

314 Superimposed to these processes there is the effect of grazers (Thompson et al. 2004), whose
315 foraging activity is known to influence either positively or negatively EMPB biomass distribution.
316 The most important grazer at the study site was *Melarhaphe neritoides*, which actively forage on
317 EMPB, leaving characteristic halos deprived of microalgae. Generally the exclusion of littorinid
318 grazers from plots of rocky substratum resulted in short-term increases of EMPB growth (Stafford
319 and Davies 2005). However, once EMPB biomass is monitored for longer periods, as in Skov et al.
320 2010, the initial positive effect of excluding snails turns out to be negative. A history of grazing by
321 *M. neritoides* can boost EMPB growth by continuously removing detritus and dead cells and, thus,
322 favouring light penetration and nutrient access.

323 Our results support the view that grazing activity is mediated by physical processes linked to
324 fresh water supply. Littorinids are more active in moist conditions, so that their impact on EMPB
325 biomass may be larger during wet days, regardless of their density (Bates and Hicks 2005). We
326 found a general positive association between grazers and D_1 at small spatial scales, suggesting that
327 grazers may generate homogenous areas of low biomass in their neighbourhoods under different
328 environmental conditions (larger D_1 values correspond to lower disorder). This positive association
329 may occasionally extend at larger scales, as observed in one transect in November 2012. However,
330 the mixed-effect model also suggested that grazing activity may result in more heterogeneous
331 spatial patterns of distribution of EMPB biomass in wet compared to dry conditions and that the
332 relation between D_1 and density of grazers is negative in the dry sampling date (January 2012) and
333 slightly positive in the wet sampling date (November 2012). Although we cannot exclude that
334 factors other than rainfall differed between sampling dates, our results strongly suggest that rainfall
335 mediates not only the effect of grazers on mean EMPB biomass, as described in other studies (Bates

and Hicks 2005, Stafford and Davies 2005, Skov et al. 2010), but also the spatial organization of EMPB distribution.

Yet, spatial self-organization may provide an alternative way to interpret our results. Spatial self-organization embraces a set of dynamical processes for which large-scale ordered spatial patterns and power law clustering distributions arise from local interactions between the components of a system (Solé and Bascompte 2006). The unifying ecological principle invoked to explain these patterns is the presence of scale-depended feedback, which emerges mainly from short-range facilitation through habitat modification and long-range competition for resources. The way this feedback acts follows Turing's scale-dependent activator-inhibitor principle (Rietkerk and van de Koppel 2008). Evidences of spatial patterns linked to scale-dependent feedback have been found in a variety of ecosystems, ranging from arid habitats (Rietkerk et al. 2002) to intertidal mudflats (Weerman et al. 2010) and mussel beds (van de Koppel et al. 2005). The power law clustering distribution of EMPB biomass that resulted in our study may underscore self-organization (Pascual et al. 2002). In EMPB communities, biofilm formation through EPS production by microalgae could be able to trigger the scale-dependent feedback required for the formation of a self-organizing pattern. Specifically, the short distance interactions of mutual benefits between microalgal cells and the large distance competitive processes for resources described before could be seen as, respectively, the activators and inhibitors of Turing's principle. In the perspective of self-organization, the strength of positive and negative feedbacks is able to mediate the action of environmental processes through mechanisms of resource concentration that take place in the activator-inhibitor systems mentioned before (Rietkerk and van de Koppel 2008). For example, across intertidal mudflats, erosive losses of microalgae by tidal flows are dampened by EPS. In a similar manner, in EMPB systems, the negative effects of adverse environmental conditions (temperature, insolation, dryness) could be mediated by EPS, which act both locally and at larger scales concentrating resources and alleviating desiccation and insolation stress.

Positive feedbacks associated with EPS were also suggested by the change in scaling regime that was evident in some of the power spectra, where the negative relation between variance and scale of observation became steeper at frequencies greater than -2.5 (on the logarithm scale). This indicated a change in autocorrelation at very small spatial scales, possibly reflecting the presence of small patches of EMPB biomass maintained by positive species interactions. The exact mechanisms underlying the observed change in scaling regime remain open to further scrutiny.

Our results have important methodological implications, emphasizing the importance of high-frequency sampling to fully capture the patterns of variability and organization of ecological variables. *In situ* remote sensing techniques facilitate this task, resulting in a large amount of data that can be analysed using multiple statistical techniques. The possibility of integrating different analytical approaches enabled us to support the hypothesis that $1/f$ noise spatial patterns are also multifractal. These results can be interpreted from two different, but not mutually exclusive perspectives. Both interpretations stress the importance of local biotic interactions, either positive or negative, in shaping spatial pattern of distribution of EMPB biomass, while differing in the way environmental processes are supposed to affect microalgal abundance. One interpretation is that environmental processes associated with temperature, insolation and moisture exert a direct effect on EMPB, determining relatively large scale variation in its biomass. In contrast, under self-organization, the influence of these abiotic variables is indirect, being mediated by the presence of the EPS matrix in which microalgal cells are embedded.

Although we did not analyze this fact, the combined use of spectral and multifractal techniques suggests, in some cases, the existence of two scaling regimes in the spatial distribution of EMPB biomass along transects. Visual inspection of a number of power spectra, indeed, could highlight that high frequencies (i.e., small spatial scales) have a higher spectral coefficient and low frequencies (i.e., large spatial scales) a lower one. Temporal tracking of changes in patch size could help discriminating between contrasting exogenous and endogenous processes influencing EMPB

386 distribution (Manor and Shnerb 2008). If, in a time series of patch size variation the probability that
387 patches shrink within a fixed time span decays exponentially with their size, the observed spatial
388 structure can be ascribed mostly to the action of physical processes, such as the topographic
389 complexity of the substratum (Vandermeer et al. 2008). If patch shrinking scales logarithmically
390 with patch size, grazing could play a major role in the clustering process (as in Kefy et al. 2007).
391 Conversely, if endogenous positive feedbacks are responsible for power law cluster distribution,
392 large clusters should disappear with a rate that depends linearly on patch size (Vandermeer et al.
393 2008). Ultimately, manipulative experiments will be required to evaluate the importance of self-
394 organization and the influence of external physical and biological processes in determining spatial
395 patterns in EMPB distribution.

396 *Acknowledgements* – We sincerely thank A. Mascellani for the support with ImageJ software and
397 several students for help with fieldwork. This work is part of a requirement for a PhD by M. Dal
398 Bello and was partially supported by the University of Pisa and by the FP 7 EU project VECTORS
399 "VECTORS of Change in Oceans and Seas Marine Life, Impact on Economic Sectors".

400 ## References

401 1. Abaimov, S. G., et al. 2007. Recurrence and interoccurrence behavior of self-
402 organized complex phenomena. – Non linear processes in geophysics 14(4): 455–464.
403 2. Agricultural Camera User's Guide. Documentation Copyright 2010 Tetracam Inc,
404 21601 Devonshire Street Suite 310 Chatsworth, CA 91311 USA.
405 3. Bates, T. W. and Hicks, D. W. 2005. Locomotory behaviour and habitat selection in
406 littoral gastropods in Caribbean limestone shores. – J. Shellfish Res. 24(1): 75–84.
407 4. Bjornstad, O. N. And Falck, W. 2001. Non-parametric spatial covariance functions:
408 estimation and testing. – Environ. Ecol. Stat. 8: 53–70.
409 5. Bodai, T. And Tel, T. 2012. Annual variability in a conceptual climate model:
410 Snapshot attractors, hysteresis in extreme events, and climate sensitivity. – Chaos 22(2):
411 023110.
412 6. Borda-de-Água, L. et al. 2007. Scaling biodiversity under neutrality. – In: Storch, D.
413 et al. (ed.), Scaling Biodiversity. Cambridge Univ. Press, pp. 347–375.
414 7. Chatfield, C. 2004. The analysis of time series: an introduction. 6th edition. – CRC
415 Press, Boca Raton, Florida, USA.
416 8. Commito, J. A. And Rusignuolo B. R. 2000. Structural complexity in mussel beds:
417 the fractal geometry of surface topography. – J. Exp. Mar. Biol. Ecol. 255: 133-152.
418 9. Denny, M. W. et al. 2004. Quantifying scale in ecology: lessons from a wave swept
419 shore. – Ecol. Monog. 74: 513–532.
420 10. Fraschetti, S. et al. 2005. Patterns of distribution of marine assemblages from rocky
421 shores: evidence of relevant scales of variation. – Mar. Ecol. Prog. Ser. 296: 13–29.
422 11. Grassberger, P. 1983. Generalized dimensions of strange attractors. – Phys. Lett. 97:
423 227–230.
424 12. Halley, J. M. and Inchausti, P. 2004. The increasing importance of 1/*f* noises as
425 models of ecological variability. – Fluctuation and Noise Letters 4(2): R1–R26.

426 13. Halley, J. M. et al. 2004. Uses and abuses of fractal methodology in ecology. – Ecol.
427 Lett. 7: 254–271.
428 14. Hausdorff, J. M. and Peng, C. -K. 1996. Multiscale randomness: A possible source of
429 noise in biology. – Phys. Rev. 54(2): 2154–2157.
430 15. Hill, A. S. and Hawkins, S. J. 1991. Seasonal and spatial variation on epilithic
431 microalgae distribution and abundance and its ingestion by *Patella vulgata* on a moderately
432 exposed rocky shore. – J. Mar. Biol. Ass. UK 71: 403–423.
433 16. Jackson, A. C. et al. 2013. Biofilms on rocky shores: Influence of rockpools, local
434 moisture and temperature. – J. Exp. Mar. Biol. Ecol. 443: 46–55.
435 17. Jordan, C. F. 1969. Derivation of leaf area index from quality of light on the forest
436 floor. – Ecology 50: 663–666.
437 18. Kefy, S. et al. 2007. Spatial vegetation patterns and imminent desertification in
438 Mediterranean arid ecosystems. – Nature 449: 213–217.
439 19. Kendal W. S. 2013. Fluctuation scaling and *1/f* noise. – J. Basic Appl. Phys. 2(2):
440 40-49.
441 20. Lomb, N. R. 1976. Least-squares frequency analysis of unequally spaced data. –
442 Astrophys. Space Sci. 39: 447–462.
443 21. Malamud, B. D. and Turcotte, D. L. 1999. Self-organized criticality applied to
444 natural hazards. – Nat. Hazards 20(2–3): 93–116.
445 22. Mandelbrot, B. 1983. The Fractal Geometry of Nature. – Freeman (Eds).
446 23. Manor, A. and Shnerb, N. M. 2008. Origin of Pareto-like distributions in ecosystems.
447 – Phys. Rev. Lett. 101: 268104.
448 24. Mendoza, F. et al. 2010. Multifractal properties of pore-size distribution in apple
449 tissue using X-ray imaging. – J. Food Eng. 99: 206–215.
450 25. Meyer, H. A. 2006. Small-scale spatial distribution variability in terrestrial tardigrade
451 populations. – Hydrobiologia 558: 133-139.

452 26. Murphy, R. J. et al. 2005. Remote-sensing of benthic chlorophyll: should ground-
453 truth data be expressed in units of area or mass? – J. Exp. Mar. Biol. Ecol 316: 69–77
454 27. Murphy, R. J. et al. 2006. Quantitative imaging to measure photosynthetic biomass
455 on an intertidal rock platform. – Mar. Ecol. Prog. Ser. 312: 45–55.
456 28. Murphy, R. J. et al. 2008. Field-based remote–sensing for experimental intertidal
457 ecology: Case studies using hyperspatial and hyperspectral data for New South Wales
458 (Australia). – Remote Sens. Environ. 112: 3353–3365
459 29. Murphy, R. J. et al. 2009. Field-based remote sensing of intertidal epilithic
460 chlorophyll: techniques using specialized and conventional cameras. – J. Exp. Mar. Biol.
461 Ecol. 380: 68–76.
462 30. Pascual, M. et al. 2002. Cluster size distributions: signatures of self–organization in
463 spatial ecologies. – Phil. Trans. R. Soc. Lond. B 357: 657–666.
464 31. Potts, M. 1999. Mechanisms of desiccation tolerance in cyanobacteria. – Eur. J.
465 Phycol. 34: 319–328.
466 32. Press, W. H. et al. 1992. Numerical recipes in Fortran 77: the art of scientific
467 computing. 2nd edition. Volume 1 of Fortran numerical recipes. – Cambridge University
468 Press, Cambridge, UK.
469 33. Rietkerk, M. et al. 2002. Self-Organization of Vegetation in Arid Ecosystems. – Am.
470 Nat. 160(4): 524–530.
471 34. Rietkerk, M. and van de Koppel, J. 2008. Regular pattern formation in real
472 ecosystems. – Trends Ecol. Evol. 23(3): 169-175.
473 35. Rodriguez, S. R. et al. 1993. Settlement of benthic invertebrates. – Mar. Ecol. Prog.
474 Ser. 97: 193–207.
475 36. Saravia, L. A. et al. 2012. Multifractal growth in periphyton communities. – Oikos
476 121: 1810–1820.

477 37. Scargle, J. D. 1982. Studies in astronomical time series analysis. II Statistical aspects
478 of spectral analysis of unequally spaced data. – Astrophys. J. 263, 835–853.
479 38. Seuront, L. and Spilmont, N. 2002. Self-organized criticality in intertidal
480 microphytobenthos patch patterns. – Physica A 313: 513–539.
481 39. Skov, M. W. et al. 2010. Past and present grazing boosts the photo-autotrophic
482 biomass of biofilms. – Mar. Ecol. Prog. Ser. 401: 101–111.
483 40. Solé, R. V. and Bascompte, J. 2006. Self-Organization in Complex Ecosystems. –
484 Princeton Univ. Press.
485 41. Stafford, R. and Davies, M.S. 2005. Spatial patchiness of epilithic biofilm caused by
486 refuge-inhabiting high shore gastropods. – Hydrobiologia 545: 279–287.
487 42. Stanley, H. E. and Meakin, P. 1988. Multifractal phenomena in physics and
488 chemistry. – Nature 335: 405–409.
489 43. Thompson, R. C. et al. 1999. Problems in extraction and spectrophotometric
490 determination of chlorophyll from epilithic microbial biofilms: towards a standard method. –
491 J. Mar. Biol. Ass. UK 79: 551–558.
492 44. Thompson, R. C. et al. 2000. Feast or famine for intertidal grazing molluscs: a
493 mismatch between seasonal variations in grazing intensity and the abundance of microbial
494 resources. – Hydrobiologia 440: 357–367.
495 45. Thompson, R. C. et al. 2004. Physical stress and biological control regulate the
496 producer–consumer balance in intertidal biofilms. – Ecology 85: 1372–1382.
497 46. Underwood, A. J. 1984. Microalgal food and the growth of the intertidal gastropods
498 *Nerita atramentosa* Reeve and *Bembicium nanum* (Lamarck) at four eights on a shore. – J.
499 Exp. Mar. Biol. Ecol. 79:277-291.
500 47. van de Koppel, J. et al. 2005. Scale-dependent feedback and regular spatial patterns
501 in young mussel beds. – Am. Nat. 165(3): E66–E77.

48. Vandermeer, J. et al. 2008. Clusters of ant colonies and robust criticality in a tropical agroecosystem. – Nature 451:457–459.

49. Weerman, E. J. et al. 2010. Spatial Self-Organization on Intertidal Mudflats through Biophysical Stress Divergence. – Am. Nat. 176(1): E15–E32.

50. Yang, J. and Wang, Y. T. 2013. Design of vascular networks: A mathematical approach. – Int. J. Numer. Method Biomed. Eng. 29(4): 515–529.

Supplementary material (Appendix oXXXXX at <www.oikosoffice.lu.se/appendix>).

Appendix 1–2–3–4.

510 Table 1. β coefficients and R^2 from linear regressions of the power spectrum of EMPB biomass
511 against frequency of observation for the two sampling dates. βs were estimated within the range of
512 frequencies defined by the Nyquist and -7 (on the natural logarithm scale). All the coefficients were
513 significantly different from zero ($p<0.001$).

Transect	Series	January 2012		November 2012	
		β (*SE*)	R^2	β (*SE*)	R^2
1(8 m)	1	1.22 (0.010)	0.79	1.02 (0.006)	0.80
	2	1.24 (0.008)	0.80	1.08 (0.005)	0.79
	3	1.33 (0.010)	0.78	0.95 (0.005)	0.79
2 (8 m)	1	1.17 (0.007)	0.82	1.61 (0.006)	0.83
	2	1.25 (0.007)	0.82	1.43 (0.006)	0.83
	3	1.24 (0.007)	0.79	1.59 (0.007)	0.81
3 (4 m)	1	1.55 (0.009)	0.77	1.39 (0.008)	0.81
	2	1.56 (0.011)	0.74	1.45 (0.009)	0.78
	3	1.64 (0.009)	0.80	1.45 (0.009)	0.80

514

515 Table 2. Mixed effect model on D_1 spatial series calculated for128 by 128 pixels plots extracted

516 from the two 8 m transects at each sampling date.

517 *, $p<0.05$

Fixed effects			
		Coefficient (*SE)*	
Intercept:	γ_{00}	$1.923\ (1.081 \cdot 10^{-2})$	***
Snail number	γ_{01}	$3.037 \cdot 10^{-4}\ (1.811 \cdot 10^{-4})$	
Rainfall	γ_{02}	$-2.093 \cdot 10^{-4}\ (1.275 \cdot 10^{-4})$	
Snail number x Rainfall	γ_{03}	$-4.767 \cdot 10^{-6}\ (2.311 \cdot 10^{-6})$	*
Random Effects		*Variances*	
Transect	σ^2_1	$5.310 \cdot 10^{-3}$	
Date	σ^2_2	$3.843 \cdot 10^{-4}$	
Quadrats apart	σ^2_3	$9.649 \cdot 10^{-8}$	
Residual	σ^2_e	$3.194 \cdot 10^{-3}$	

518

519 LEGEND TO FIGURES

520 Figure 1. Sampling within transects. **A**, a section of a transect obtained from the merging of
521 individual photos. The white chalk marks at the corners of each plot and the reflectance standard are
522 visible in all the photos. **B** and **C**, spatial arrangement of sampled pixels. Crosses show the position
523 of chalk marks that were used to align overlapping photos. Vertical black and grey dotted lines
524 delimit the margins of the right-hand and left-hand photos in each pair of adjacent photos and define
525 the region of overlap. Circles represent the reflectance standard. **B,** horizontal black lines represent
526 the three series of observations used in $1/f$ noise analysis that were aligned along a common y
527 coordinate; data from pixels in the overlapping regions (horizontal grey lines) were not used in the
528 analysis; size of gaps in the region of overlap is measured in pixels. **C**, spatial arrangement along a
529 common y coordinate of the five adjacent plots (128 by 128 pixels each) used in the multifractal
530 analysis (black quadrates). Grey quadrates within regions of overlap have not been used in the
531 analysis.

532 Figure 2. Calibration curve: chlorophyll *a* concentration determined from laboratory analysis
533 ($\mu g \cdot cm^{-2}$) versus image estimates of chlorophyll from sandstone cores (Ratio Vegetational Index,
534 RVI), R^2= 0.80, SE=0.12, p<0.001, n=100.

535 Figure 3. Spectrum of generalized dimensions D_q versus q obtained for the 1024 by 1024 sampled
536 plots separately for transect 1, 8 m long, n= 11 (A), transect 2, 8 m long, n= 18 (B) and transect 3, 4
537 m long, n= 10 (C).

538 Figure 4. Interactive effect of the snails density and average rainfall in the week before the sampling
539 on mean D_1 (n=64, means ± standard errors). White, average rainfall: 0 mm; gray, average rainfall:
540 110 mm.

541 Figure 5. Spatial cross-correlation between littorinid density and D_1 in each of two 8m transects
542 sampled in January 2012 (A, B) and November 2012 (C, D). D_1 values have been obtained from 64

543 quadrats of 128 x 128 pixels aligned along a common y coordinate, but unevenly spaced along each
544 transect. Note that these quadrats did not span the entire length of a transect as a consequence of
545 avoiding portions of substratum that would have resulted in non-sense measures of EMPB biomass
546 (e.g., shaded areas due to crevices).

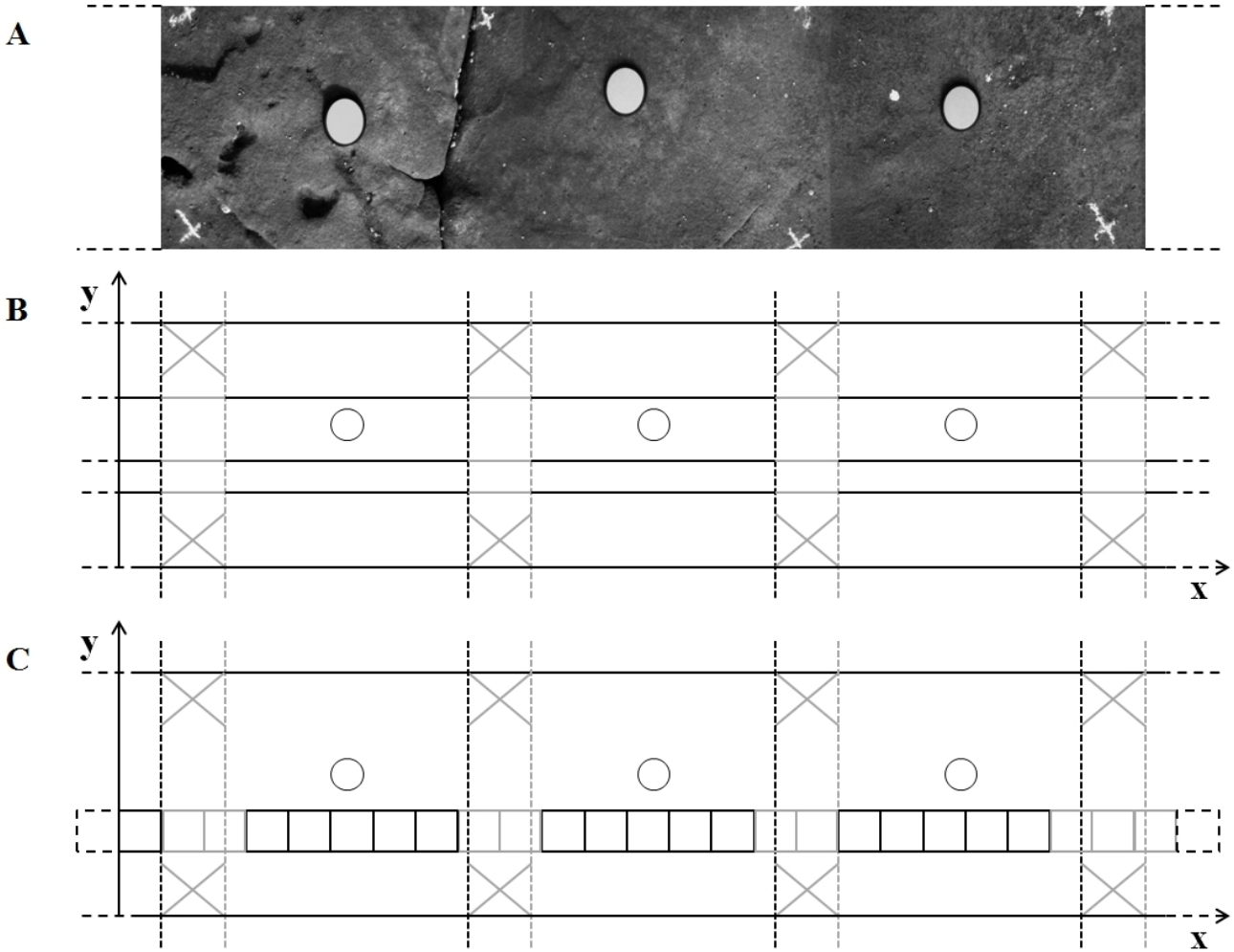

Dal Bello et al. Figure 1.

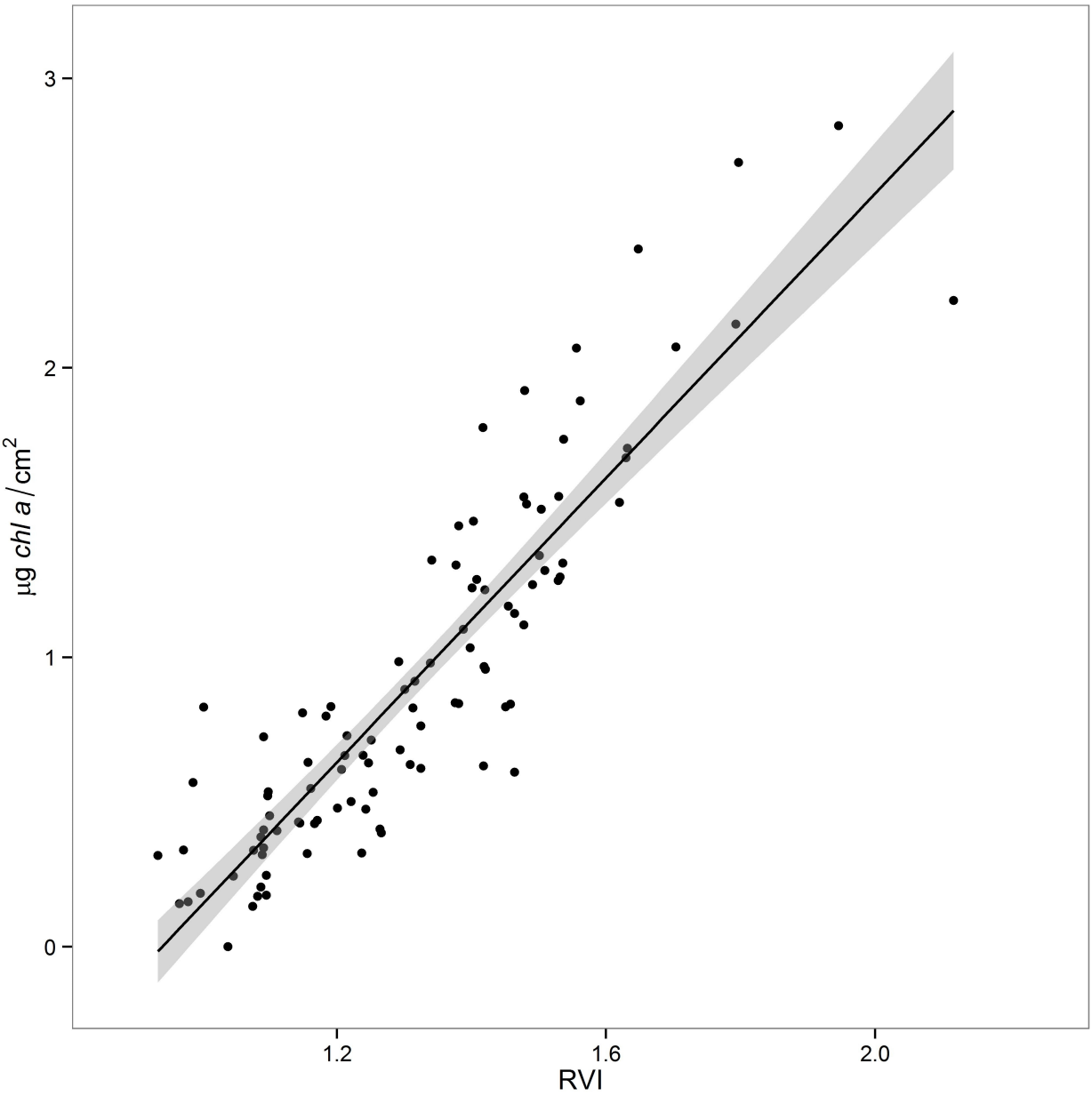

Dal Bello et al. Figure 2.

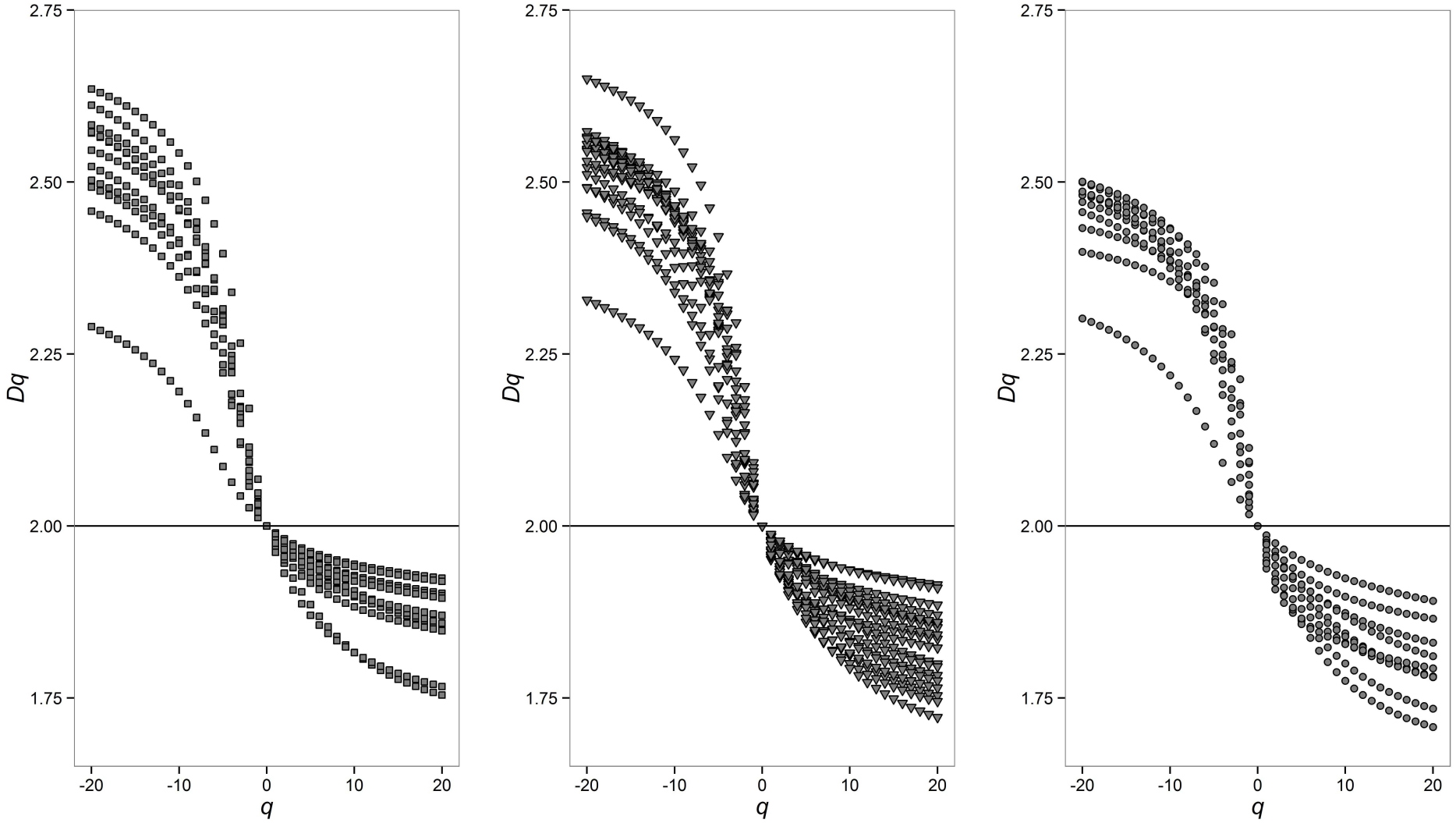

Dal Bello et al. Figure 3.

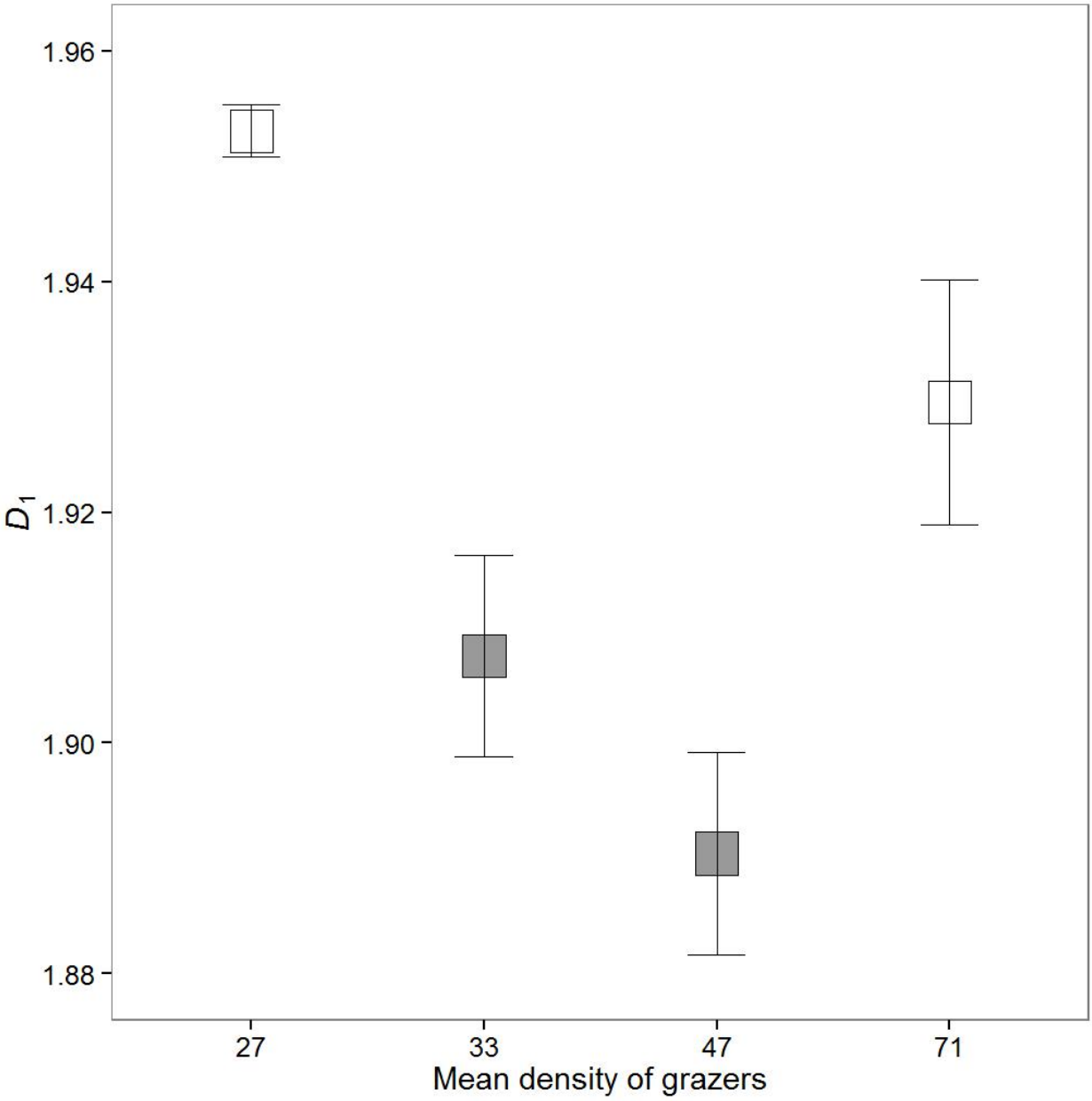

Dal Bello et al. Figure 4.

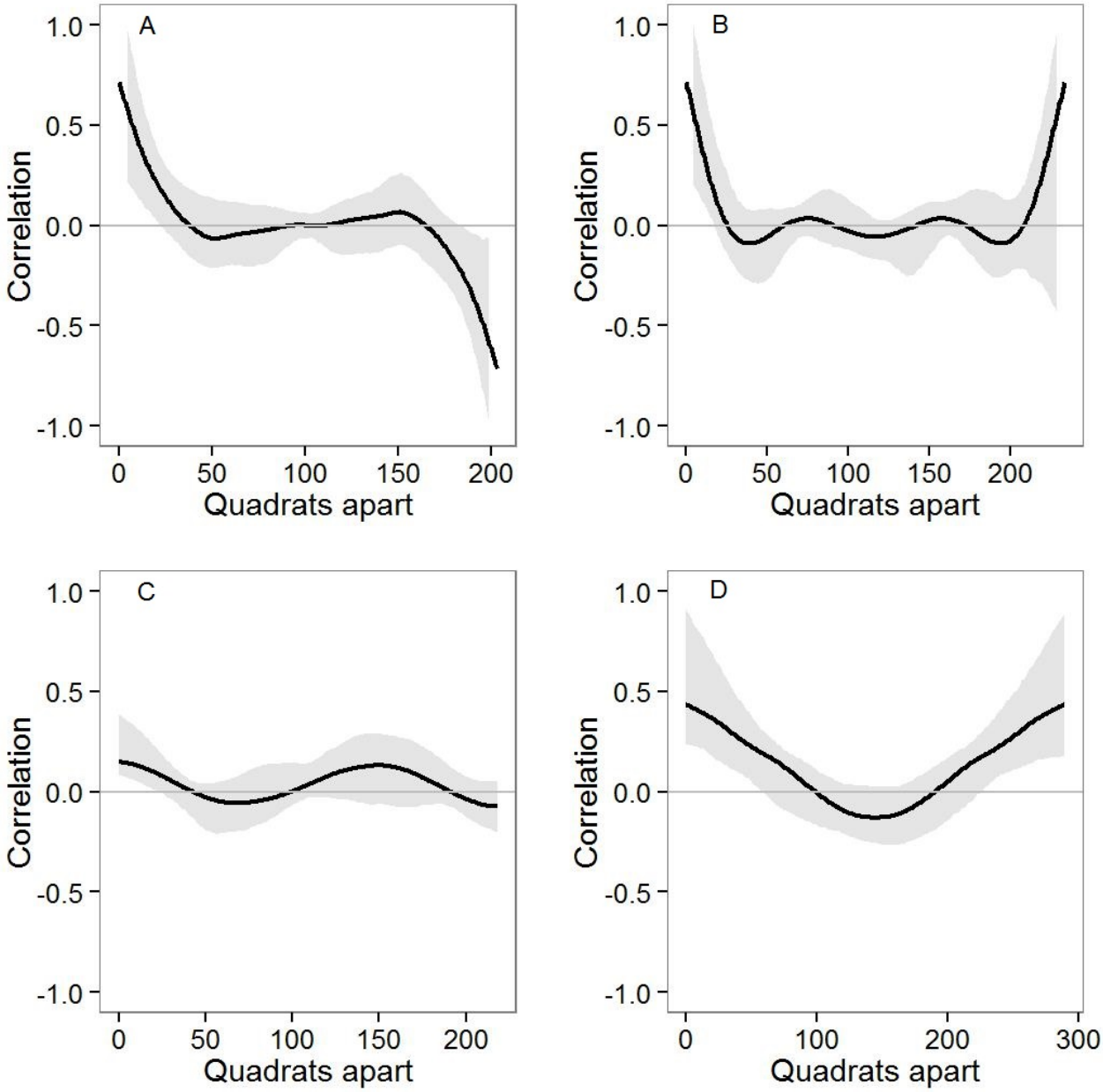

Dal Bello et al. Figure 5.

Appendix 1.

Calibration of data to reflectance

Pixel values (Digital Number, *DN*) over the calibration standard are averaged and the reflectance (ρ) for each band in each photo is calculated as

$$\rho(photo) = \frac{DN(photo)\rho(panel)}{DN(panel)}$$

where $\rho(photo)$ is the reflectance at each pixel in the photo; $\rho(panel)$ is the reflectance of the calibration standard, which is a known constant; $DN(photo)$ is *DN* at each pixel in the photo and $DN(panel)$ is the average *DN* of the pixels over the calibration standard (Murphy et al. 2006). Calibration is part of a java-routine on ImageJ program with which each ADC-photo is processed. Calibration of data to reflectance is of fundamental importance when one wants to compare chlorophyll amounts estimated from photos acquired at different times and places.

References

Murphy, R. J. et al. 2006. Quantitative imaging to measure photosynthetic biomass on an intertidal rock platform. – Mar. Ecol. Prog. Ser. 312: 45–55.

Appendix 2

Calculation of the generalized dimension spectrum D_q

Generalized dimensions are exponents estimated by the box counting method: the plot is covered with a grid of $N(\varepsilon)$ squares of side ε and for each square a value of standardized biomass is calculated as

$$M_i(q,\varepsilon) = \frac{(\mu_i(\varepsilon))^q}{\sum_j^{N(\varepsilon)}(\mu_j(\varepsilon))^q}. \quad (1)$$

where μ is the measured biomass and q is called the moment order and can be considered an arbitrary exponent. An adjustment corresponding to +(minimum observed biomass)/100 has been applied to all biomass values before the standardization in order to avoid zeros.

Then the partition function is computed as:

$$Z_q(\varepsilon) = \sum_i^{N(\varepsilon)}(M_i(q,\varepsilon)). \quad (2)$$

The operation is performed for different values of ε and q. In order to exactly divide the plots, a grid size range of ε in power of two with a minimum of 2^2=4 and a maximum of 2^7=128 or 2^{10}=1024 pixels was chosen; the q exponent ranged between -20 and +20.

The generalized dimension is calculated as:

$$D_q = \frac{1}{q-1}\lim_{\varepsilon\to 0}\frac{\log(Z_q(\varepsilon))}{\log\ \varepsilon}. \quad (3)$$

This limit cannot be determined. Hence the second term in D_q is calculated as the slope of the regression of $\log(Z_q)$ versus $\log(\varepsilon)$. A linear relation is assumed, which is estimated using the least squares method.

For q=1, the denominator of the first term in D_q is undefined, so Eq. 3 is replaced by:

$$\lim_{\varepsilon\to 0}\frac{\sum_i^{N(\varepsilon)}\mu_i(\varepsilon)\log(\mu_i(\varepsilon))}{log\varepsilon}. \quad (4)$$

To see that D_q is actually an exponent, Eq. 3 can be rearranged to obtain:

$$Z_q \approx\ \varepsilon^{D_q(q-1)}\ . \quad (5)$$

Eq. 5 determines how Z_q varies with the scale ε and it is evident that it is a power law.

Details of results

We found a linear relation between $\log(Z_q)$ and $\log(\varepsilon)$ for all plots sampled and all q used. As a measure of goodness of fit, we calculated the coefficient of determination R^2, which was always larger than 0.99.

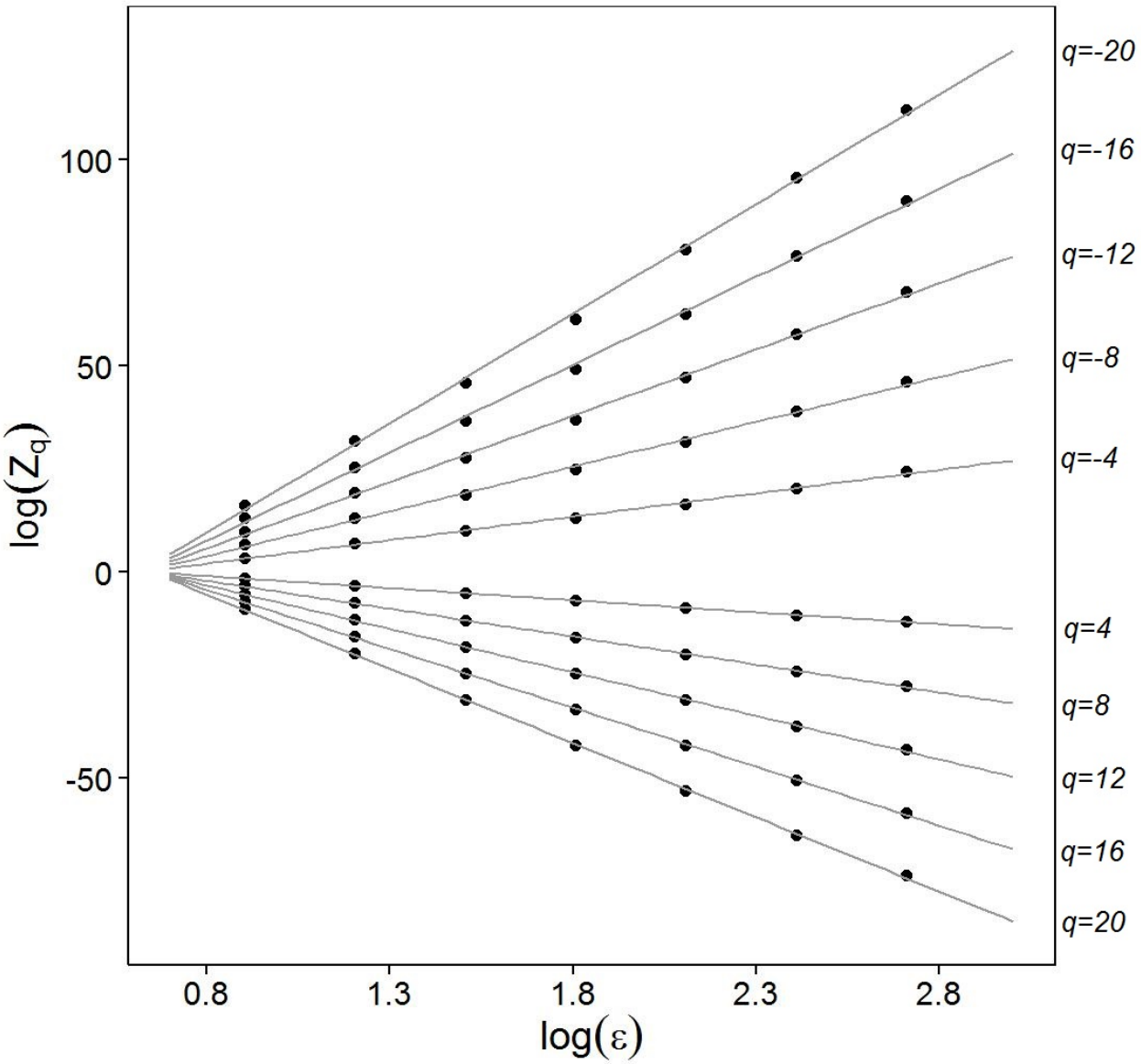

Figure A2.1. Example of a typical graph for the determination of the generalized dimension D_q for one subplot 1024 by 1024 pixels. It shows all the regression lines for ten values of q.

Appendix 3

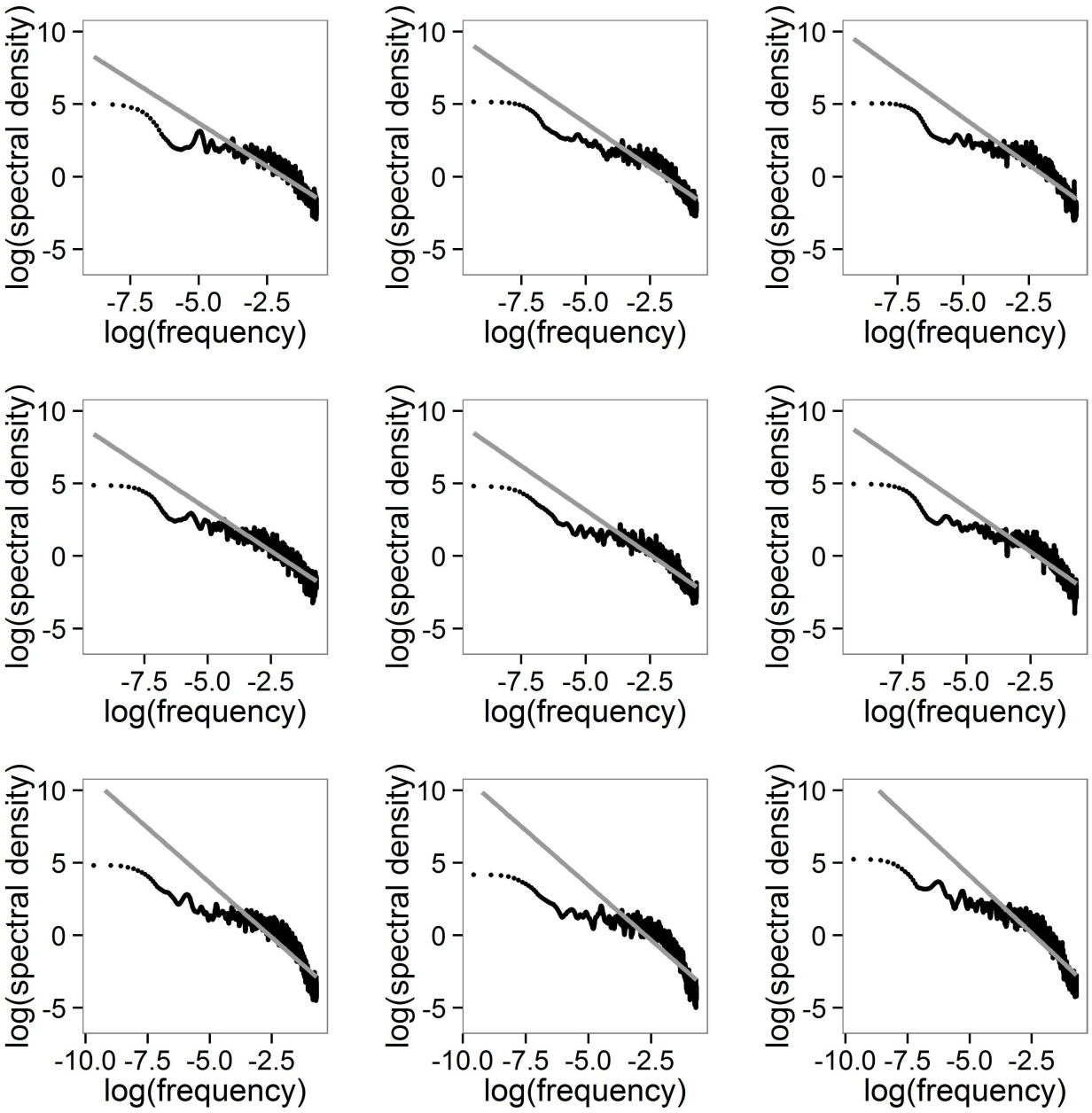

Figure A3.1. Power spectra of EMPB biomass separately for each transect. The spectral density is plotted against frequency of observation (pixel^{-1}) on a natural log-log scale. Data are from the first date of sampling (26.01.2012).

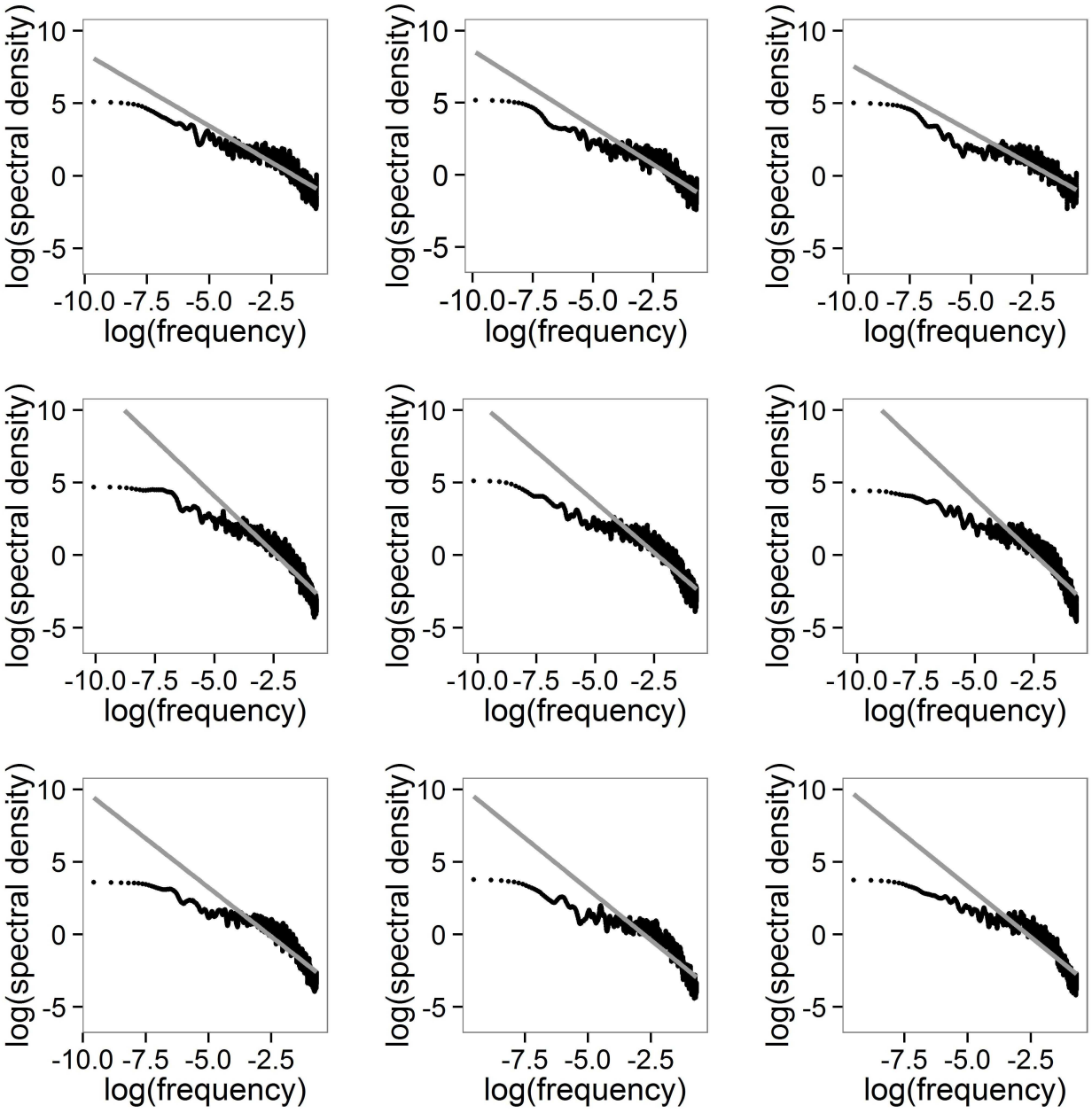

Figure A3.2. Power spectra of EMPB biomass separately for each transect. The spectral density is plotted against frequency of observation (pixel^{-1}) on a natural log-log scale. Data are from the second date of sampling (16.11.2012).

Appendix 4

Table A4.1. β coefficients and R^2 from linear regressions of the power spectrum of EMPB biomass data obtained from quadrats of 80 x 80 pixels against frequency of observation for the two sampling dates. All the coefficients were significantly different from zero ($p<0.001$).

Transect	Series	January 2012		November 2012	
		β (*SE*)	R^2	β (*SE*)	R^2
1	1	1.71 (0.050)	0.92	0.88 (0.036)	0.80
	2	1.29 (0.058)	0.82	0.97 (0.033)	0.88
2	1	1.11 (0.034)	0.90	0.76 (0.045)	0.66
	2	1.35 (0.039)	0.91	0.86 (0.045)	0.71
3	1	1.17 (0.070)	0.72	1.36 (0.052)	0.86
	2	1.27 (0.050)	0.77	1.16 (0.054)	0.81